In situ study on the thermal stability of supported Pt nanoparticles and their stabilization via Atomic Layer Deposition overcoating

Reference

E. Solano, J. Dendooven, J.-Y. Feng, P. Brüner, M. M. Minjauw, R. K. Ramachandran, M. Van Daele, K. Van de Kerckhove, T. Dobbelaere, A. Coati, D. Hermida-Merino and C. Detavernier, Nanoscale **12** (21), 11684-11693 (2020).

Full text (Publisher's DOI): https://doi.org/10.1039/D0NR02444A

Nanoscale

Accepted Manuscript

This article can be cited before page numbers have been issued, to do this please use: E. Solano, J. Dendooven, J. Feng, P. Brüner, M. M. Minjauw, R. K. Ramachandran, M. Van Daele, K. Van de Kerckhove, T. Dobbelaere, A. coati, D. Hermida Merino and C. Detavernier, *Nanoscale*, 2020, DOI: 10.1039/D0NR02444A.

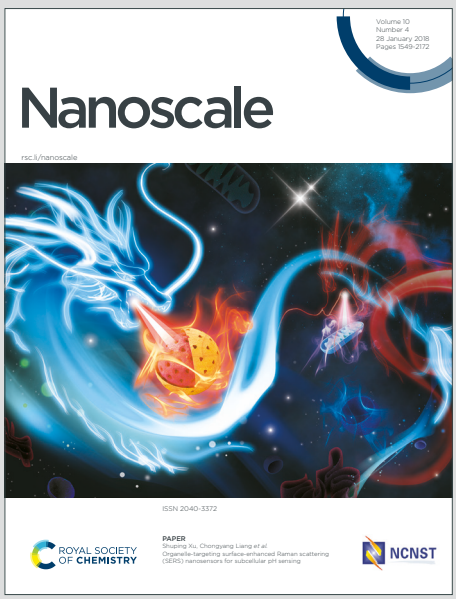

ROYAL SOCIETY OF CHEMISTRY

rsc.li/nanoscale

View Article Online
DOI: 10.1039/D0NR02444A

Journal Name

ARTICLE TYPE

Cite this: DOI: 00.0000/xxxxxxxxxx

In situ study on the thermal stability of supported Pt nanoparticles and their stabilization via Atomic Layer Deposition overcoating†

Eduardo Solano,*[a,b‡] Jolien Dendooven,[b‡] Ji-Yu Feng,[b] Philipp Brüner,[c] Matthias M. Minjauw,[b] Ranjith K. Ramachandran,[b] Michiel Van Daele,[b] Kevin Van de Kerckhove,[b] Thomas Dobbelaere,[b] Alessandro Coati,[d] Daniel Hermida-Merino[e] and Christophe Detavernier[b]

Received Date
Accepted Date

DOI: 00.0000/xxxxxxxxxx

Downscaling supported Pt structures to the nanoscale is motivated by the augmentation of the catalytic activity and selectivity, which depend on the particle size, shape and coverage. Harsh thermal and chemical conditions generally required during catalytic applications entail an undesirable particle coarsening, limiting as consequence the catalyst lifetime. Here we report an *in situ* synchrotron study on the stability of supported Pt nanoparticles using Atomic Layer Deposition (ALD) as stabilizing methodology against particle coarsening. Pt nanoparticles were thermally annealed up to 850 ^{o}C in an oxidizing environment while recording *in situ* synchrotron Grazing Incidence Small Angle X-ray Scattering (GISAXS) 2D patterns, obtaining continuous information about the particle radius evolution. Al_2O_3 overcoating as protective capping layer against coarsening via ALD was investigated. *In situ* data proved that only 1 cycle of Al_2O_3 ALD caused an augmentation of the onset temperature for particle coarsening. Moreover, results showed a dependence of the required overcoating thickness on the initial particle size and distribution, being more efficient (i.e. requiring lower thicknesses) when isolated particles are present on the sample surface. The Pt surface accessibility, which is decisive in catalytic applications, was analyzed via Low Energy Ion Scattering (LEIS) technique, revealing a larger Pt surface accessibility for a sample with Al_2O_3 overcoating than for a sample without protective layer after a long isothermal annealing.

1 Introduction

Downscaling supported Pt structures is of interest for well-established catalytic applications (e.g. automotive exhaust[1,2] and industrial catalysis[1,3–5]) as well as for emerging technologies (e.g. fuel cells for electrochemical conversion[6,7]). This interest is motivated by the high particle catalytic activity and selectivity of atoms, clusters and nanoparticles, which depends on the number, location, and density of the active sites and hence, on the particle size, shape and coverage[8,9]. Moreover, nanoparticles present advantages over single atom catalysts or clusters for potential applications, since limitations exist when downscaling towards single atom catalysts, e.g. atoms could act as spectator contrarily to clusters or nanoparticles.[10]

Industrial applications using nanoparticles often require harsh thermal and chemical conditions, which are known to favor particle coarsening[11–13], forming larger and more stable structures, lowering the amount of active sites, and as a consequence precluding the interesting properties of Pt at the nanoscale[14,15]. In fact, we reported an *in situ* synchrotron study where the stability and mechanism governing the coarsening of supported Pt nanoparticles under hash thermal and oxidizing conditions was investigated[11]. The investigation showed that for a given Pt loading, smaller (and denser) nanoparticles presented a lower onset temperature for particle coarsening, while larger particles showed a higher thermal stability. It was also proven that the particle sta-

[a] *NCD-SWEET beamline, ALBA Synchrotron Light Source, Carrer de la Llum 2-26, 08290 Cerdanyola del Vallès, Spain.*
[b] *Department of Solid State Sciences, CoCooN, Ghent University, Krijgslaan 281/S1, 9000 Ghent, Belgium.*
[c] *IONTOF Technologies GmbH, Heisenbergstr. 15 48149 Muenster, Germany.*
[d] *SIXS beamline, Synchrotron SOLEIL, L'Orme des Merisiers Saint-Aubin BP 48 91192 Gif-sur-Yvette, France*
[e] *DUBBLE beamline, ESRF, Avenue des Martyrs 71, 38000 Grenoble, France*
‡ *E.S. and J.D equally contributed to this work.*
* *Corresponding author: esolano@cells.es*
† Electronic Supplementary Information (ESI) available: See DOI: 10.1039/b000000x/

View Article Online
DOI: 10.1039/D0NR02444A

bility depends on the O_2 concentration, since the decomposition of a formed PtO_2 layer plays a pivotal role in triggering the particle coarsening.

Therefore, large efforts and resources have been invested to prevent coarsening of the Pt catalyst particles under harsh thermal and oxidative conditions, emulating realistic catalytic environments. Diverse stabilization approaches have been proposed including trapping[16], doping[17,18], isolation[19] and encapsulation[20] among others[14]. In recent years, particle overcoating has attracted the interest of the scientific community for preventing the coarsening of supported nanostructures[21–25]. This methodology is based on the deposition of a protecting layer over the support and particles, trapping the nanoparticles in between the substrate and the capping layer[26]. To ensure Pt surface accessibility for applications of interest, a thermal treatment has demonstrated to produce an increment of the overcoating layer porosity[22] by cracks formation[26,27]. This phenomenon introduces canals that divide the noble metal surface in isolated units, which are too small for sintering and coke formation but accessible enough for a catalytic process, preventing in this way catalyst coarsening and poisoning[21,28].

Therefore, to fundamentally study the efficiency of an overcoating layer for particle coarsening prevention during a thermal annealing, fundamental *in situ* investigations are required. Synchrotron Grazing Incident Small Angle X-ray Scattering (GISAXS) has been highlighted as a powerful and precise technique to investigate supported nanoparticles under realistic working conditions[11,29,30]. GISAXS provides information on spatial correlation and morphological properties of nanometric or submicrometric structures at surfaces, buried interfaces or thin films[31,32]. It is based on the scattering of a collimated and narrow incident X-ray beam caused by electronic inhomogeneities on the probed material. Therefore continuous area-averaged lateral and normal information of the supported nanostructures can be obtained during a process of interest when using GISAXS as *in situ* characterization tool.

This work presents an *in situ* synchrotron GISAXS study to investigate the stability and evolution of supported Pt nanoparticles during thermal annealing when using ALD overcoating to prevent particle coarsening. The dependence of the overcoating layer thickness with respect to the initial nanoparticles size and coverage will be assessed. Moreover, since molecular access to the surface of the supported nanoparticles is crucial for catalytic purposes, Pt surface accessibility after overcoating will be proved.

2 Experimental section

2.1 Sample preparation

2.1.1 Fabrication of supported Pt nanoparticles

Supported Pt nanoparticles were prepared following a procedure described elsewhere[11,30]. Two different samples containing the same amount of Pt, but distinct as-deposited particle size and coverage were fabricated profiting the distinct nucleation regime of the O_2 and N_2 plasma (N_2*) Pt ALD processes[30]. In brief, Pt nanoparticles were deposited on a -OH terminated Si (100) wafer heated to 300 ^{o}C in a pump-type ALD reactor[33]. The chamber base pressure was $1{\cdot}10^{-6}$ mbar. Prior to the ALD process, the Si surface was exposed to 30 s of O_2 plasma (200 W) in order to ensure a complete removal of possible organic contaminants, augmenting the reproducibility of the deposition. Then, the sample was exposed to a certain number of cycles comprising alternating injection of the Pt precursor, i.e. (methylcyclopentadienyl)trimethylplatinum($MeCpPtMe_3$) 99 % (Strem Chemicals) and a reactant, i.e. O_2 gas or N_2 plasma. The precursor was injected during 5 s up to 1 mbar, followed by 9 s of dwell time, while the reactant, i.e. O_2 gas or N_2* (200 W) was injected during 9 s with a constant pressure of $5{\cdot}10^{-3}$ mbar. Between pulses, the gases were evacuated from the chamber, reaching base pressure. Ar was used as carrier for the Pt precursor, which was heated to 30 ^{o}C in a vacuum sealed container.

Two samples were fabricated using 40 cycles of O_2-based Pt ALD and 30 cycles of N_2*-based Pt ALD respectively, resulting in samples with a similar amount of deposited Pt ($5.35{\cdot}10^{15}$ and $5.85{\cdot}10^{15}$ at./cm^2 respectively) but distinct particle size (particle radius of 3.2 nm and 2.1 nm respectively) and thus, coverage (11.8 and 6.2 nm of average particle center-to-center distance respectively).

2.1.2 Laboratory characterization

Scanning Electron Microscopy (SEM) real-space images were acquired using a FEI Quanta 200 F with an electron acceleration voltage of 20 kV. The backscattered electrons were detected using an Everhart-Thornley detector (i.e. an scintillator placed in a Faraday cage). **X-ray fluorescence** spectra were recorded using a Bruker Artax instrument with a Mo X-ray source (0.7107 Å) and a Silicon drift detector using 100 s of acquisition time. The Pt loading was determined by integrating the Pt L_α peak and by refereeing the integrated counts of the Pt L_α line against an established XRF-Rutherford Backscattering Spectroscopy (RBS) calibration curve[30]. **Low Energy Ion Scattering** (LEIS) *Ex situ* low energy ion scattering (LEIS) spectra were recorded using an IONTOF Qtac 100 instrument equipped with a double toroidal analyzer with full azimuthal acceptance. The polar scattering angle was fixed at 145°, using a normal incidence primary ion beam. Prior to the analysis, each sample was cleaned in vacuum by exposure to atomic oxygen extracted from a plasma source. This cleaning procedure removes any organic adsorbents from transport through air and fully oxidizes the surface. Particle thickness measurements were performed by measuring the energy loss of6 keV scattered He^+ ions. ions scattered in the bulk of the nanoparticles. The maximum energy loss was converted to particle thickness by using the stopping power of He^+ ions in Pt obtained from the SRIM software[34]

2.1.3 *In situ* GISAXS during thermal annealing

Sample overcoat via ALD and the subsequent thermal treatment were carried out in a dedicated chamber designed for *in situ* experiments[33]. The sample to be annealed was placed on a specific heater controlled with a Eurotherm PID regulator. In order to ensure a high purity annealing atmosphere, a base pressure of $1{\cdot}10^{-6}$ mbar was reached before any treatment. Then, if required, the sample was overcoated with an Al_2O_3 layer with a

View Article Online
DOI: 10.1039/D0NR02444A

defined number of ALD cycles. For that, the sample was exposed to several cycles of trimethylaluminum (TMA) (Strem Chemicals) and H_2O. The pressure and exposure time were $5{\cdot}10^{-3}$ mbar and 5 s for both, precursor and reactant. Between pulses, a base pressure of $1{\cdot}10^{-6}$ mbar was reached. The sample temperature was 150 °C during the ALD process. After overcoating, the sample was cooled down to room temperature, while the chamber was at base pressure. The chamber was filled up to 1 bar with a mixture of 18 % O_2 (99.999 %) in He (99.999 %) using a continuous flow of 500 sccm set by a Mass Flow Control system. Then, the thermal treatment was carried out up to 850 °C, at a ramp rate of 0.2 °C/s, while continuous GISAXS images were being recorded.

2.1.4 *In situ GISAXS*

In situ GISAXS experiments were performed at the SixS beamline of synchrotron SOLEIL (Gif-sur-Yvette, France) and at the BM26B beamline of the ESRF (Grenoble, France). The annealing chamber was placed on the aligment device available at the respective beamline end stations, i.e. a hexapod situated on a diffractometer at SixS ans a pillar at BM26B beamline, allowing precise movements and tilts along the three x-y-z spatial directions[33]. The beam energy was set to 12 keV by using a Si(111) double-crystal monochromator. The beam size at SixS [BM26B] was 400 × 100 [1000 × 400] μm^2 FWHM. The selected X-ray incident angle was 0.5^o for all the experiments. The scattered radiation was recorded using either an Eiger 1M detector (Dectris Ltd., Switzerland) with an array dimension of 1030 × 1065 pixels, pixel size of 75 × 75 μm^2 placed at 1050 mm from the sample position at SixS or using a Pilatus3S 1M detector (Dectris Ltd., Switzerland) with an array dimension of 1043 × 981 pixels, pixel size of 172 × 172 μm^2 placed at 4665 mm from the sample position at BM26B. Continuous GISAXS images were recorded during the annealing experiments with 10 s of integration time at SixS and 30 s at BM26B.

2.2 Data analysis

Analysis of the recorded GISAXS scattering patterns was achieved using a computing routine which was applied to each of the recorded GISAXS images[11]. Horizontal intensity cuts (I(q) vs q_y) at the Si Yoneda peak were extracted integrating 5 pixels which defines the scattering peak position. Horizontal cuts were fitted to a Gaussian peak, extracting the peak position with a confidence interval of 95 %. The average center-to-center distance between scatterers (D) was calculated using the $D = \frac{2\pi}{q_{y,max}}$ approximation. Knowing the amount of deposited Pt on the surface (determined via XRF analysis calibrated with RBS[30]), the average equivalent spherical radius (R) was calculated using equation (1), with D the average distance between scatterers, S_{Pt} the Pt surface density (calculated via XRF) and using the bulk Pt density (66.24 at./nm^3).

$$D(nm) = \sqrt{\frac{\frac{4}{3}\pi R^3 \cdot 66.24(at./nm^3)}{S_{Pt}(at./nm^2)}} \quad (1)$$

Data were extracted from all the patterns recorded during the *in situ* annealing experiments, obtaining continuous information about the particle size evolution during the thermal annealing experiments.

3 Results and discussion

3.1 As-deposited samples analysis

Fig. 1 depicts the fabrication and as-deposited details of the two samples under study. The scattered radiation (GISAXS patterns) presented a distinct $q_{y,max}$ peak position and morphology, indicating a different average distance between the scatterers for the two samples: Pt nanoparticles deposited using O_2 (Pt-O) as reactant presented a larger average D distance (11.8 nm) compared to the samples prepared via N_2* (Pt-N) process (6.2 nm). Knowing the amount of deposited Pt employing XRF, and using a calibration XRF-RBS curve[30], a spherical equivalent average particle radius of 3.2 and 2.1 nm was obtained for the Pt-O and Pt-N samples, respectively. The presence of a secondary lobe at lower q_z values for the Pt-O sample corroborates the larger particle size when compared to the Pt-N supported nanoparticles. Moreover, GISAXS simulations, presented in previous publications[11,30], revealed a difference in nanoparticle shape for the two processes. The best agreement between the experimental and simulated GISAXS patterns was found for hemiellipsoids and ellipsoids for the O_2-based and N_2*-based processes respectively. Scanning Electron Microscopy (SEM) was employed as a complementary tool, offering real-space information. The images in Fig. 1 confirmed GISAXS results on the differences in the as-deposited particle size and coverage.

3.2 *In situ* thermal annealing of as-deposited samples

The prepared samples (Pt-O & Pt-N) were annealed under 18 % O_2 in He up to 850 °C (0.2 °C/s) while recording *in situ* GISAXS patterns. Fig. 2 presents a selection of the continuously recorded GISAXS images at different temperatures (2a). The 2D GISAXS pattern evolution during the treatment demonstrated a higher thermal stability of the Pt-O nanoparticles, since there was not any evident change below 500 °C. Contrarily, the recorded Pt-N GISAXS images showed a variation of the pattern below 500 °C, as observed in Fig. 2a.

Through the extraction of the main peak $q_{y,max}$ position during the experiment, it was possible to extract the equivalent spherical particle radius evolution during the thermal treatment. Fig. 2b depicts the particle radius evolution as a function of the sample temperature for the as-deposited Pt nanoparticles. These data allow to determine the onset temperature for particle coarsening using the maximum of the second derivate, being ∼ 478 °C [∼ 574 °C] for the Pt-N [Pt-O] sample. Moreover, when increasing the temperature, both samples (with equivalent Pt loading but distinct as-deposited particle size and distribution) followed a similar evolution trend from ca. 650 °C and above. This particle radius evolution is in agreement with a previously reported work[11]. In that investigation, we argued that the particle evolution during thermal treatment under O_2 atmosphere presents three different regimes as a function of the temperature, whose temperature window depends on the particle size and O_2 partial pressure for a given Pt loading:

I Particle stability: no particle growth was observed when the

View Article Online
DOI: 10.1039/D0NR02444A

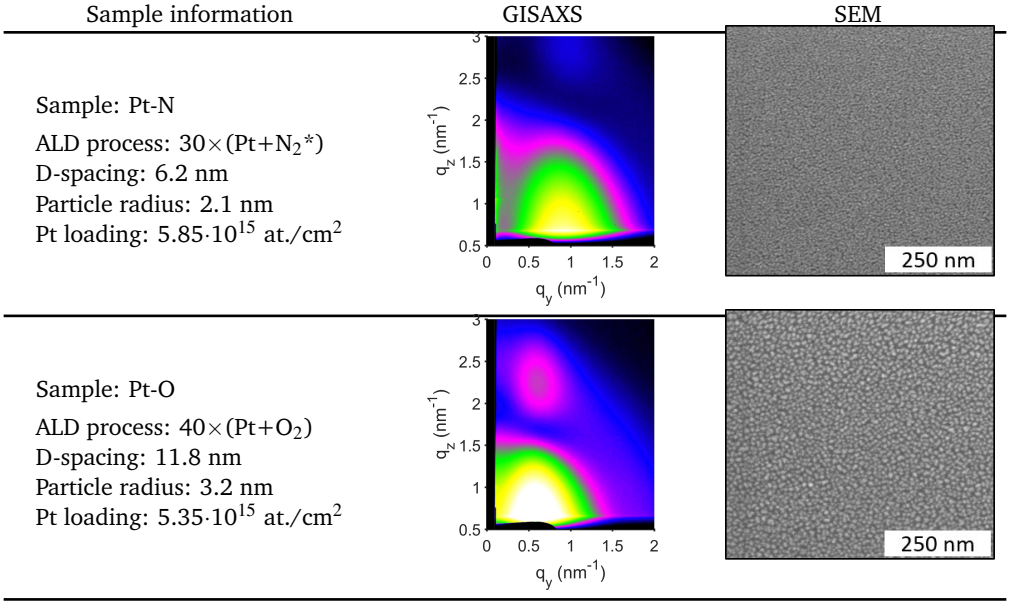

Fig. 1 Overview of the as-deposited samples. D-spacing and particle radius were obtained from the acquired GISAXS pattern. Differences on the scattering $q_{y,max}$ GISAXS lobe position indicated the different D spacing between the two samples. SEM images verified in real space the differences on the particle size and coverage between the as-deposited supported Pt-N and Pt-O nanoparticles.

samples were subjected to a moderate temperature (stage I). However, under an oxidizing environment (i.e. O_2 18 % in He), a potential surface oxidation occurs, which would create a PtO_2 shell that would cover the Pt surface. This shell is thought to stable under the applied conditions.

II Coarsening: when the onset temperature for coarsening is surpassed, a thermal decomposition of the superficial PtO_2 shell would likely occur, forming unstable and mobile PtO_x species that would further decompose into metallic Pt. These oxide species could act as Pt transport agents between particles via the Ostwald ripening mechanism (stage II). Because of the O_2 presence at high temperature, the PtO_2 could be regenerated, enabling the formation of more mobile PtO_xspecies that would contribute to the Ostwald ripening. *In situ* data[11] proved that for low O_2 concentrations, the particle radius increases when augmenting the temperature until a steady-state is reached, where no further particle growth was observed: the particles reach a stable size and distribution, presenting a quasi-equilibrium where the amount of emitted and received Pt atoms by a single particle would be equivalent, having a zero net mass transfer[11]. However, if the O_2 concentration is high enough (as during the present experiments) the steady-state was not observed since the coarsening process entered into the phase III before reaching stability.

III Reactivation: by increasing the temperature, PtO_2 desorption from the particle surface occurs, as we proved via XRF[11]. The PtO_2 evaporation could affect to the system stability by a local diminishment of the particle size, whose instability would augment and therefore, the Ostwald ripening process could be favored and enhanced, augmenting the coarsening growth rate (stage III). The onset temperature for desorption was proved to depend on the O_2 concentration and Pt loading, but not on the initial particle size, since both samples presented a similar temperature for the phase II-III transition, being ~650 °C.

Pt-N process	Al_2O_3 cycles	Pt-O process	Al_2O_3 cycles
	0 cycles		0 cycles
	1 cycle		1 cycle
30×(Pt+N_2*)	5 cycles	40×(Pt+O_2)	3 cycles
	10 cycles		5 cycles
	20 cycles		10 cycles
	40 cycles		

Table 1 Overview of the prepared Pt-N and Pt-O samples with different Al_2O_3 overcoat cycles.

3.3 Al_2O_3 overcoating and *in situ* thermal annealing

To determine the effect of different Al_2O_3 overcoat thicknesses on the particle stability during thermal annealing, *in situ* GISAXS patterns were recorded right after the overcoating procedure, exposing the sample only to the annealing atmosphere. The two investigated samples, i.e. Pt-N and Pt-O, were overcoated with different thicknesses of Al_2O_3 via ALD prior to the sample annealing up to 850 °C (0.2 °C/s) in O_2 18 % in He. Table 1 summarizes the different samples prepared and annealed.

In situ GISAXS images recorded during the annealing procedure (Fig. S1 and Fig. S2) were analyzed following the above-mentioned data analysis procedure[11], obtaining the continuous evolution of the particle size during the experiment. Results are summarized in Fig. 3, which depicts the evolution of the Al_2O_3 overcoated Pt nanoparticles during the annealing procedure up to 850 °C under the selected oxidizing atmosphere. The effect of

View Article Online
DOI: 10.1039/D0NR02444A

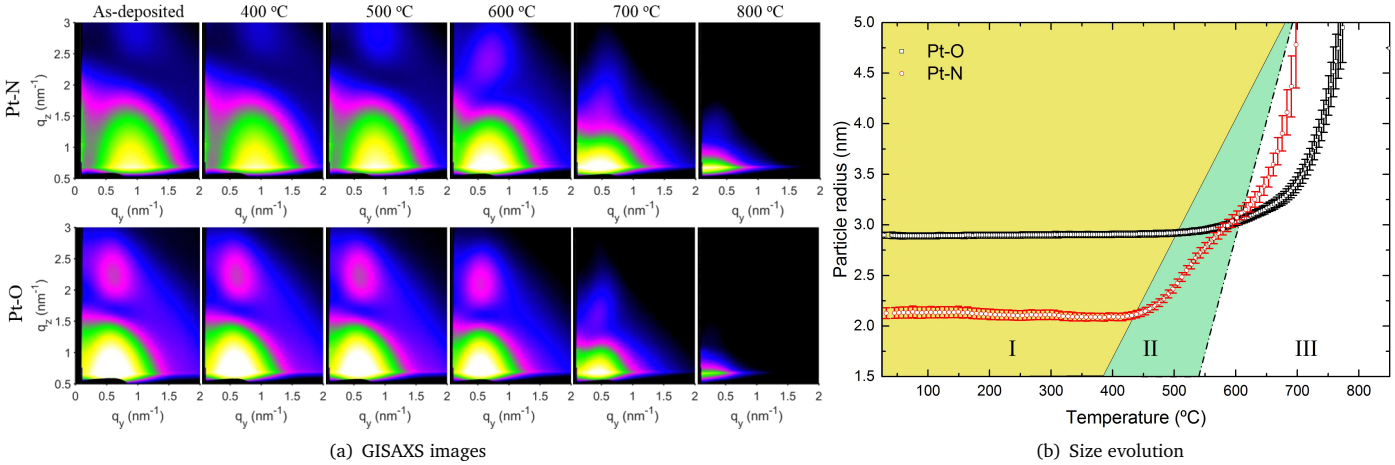

(a) GISAXS images (b) Size evolution

Fig. 2 (a) Selection of the acquired *in situ* GISAXS patterns for both initial Pt morphologies (without any overcoat) at different temperatures during the annealing procedure up to 850 °C (0.2 °C/s) in 18 % O_2 in He. Differences on the as-deposited scattering patterns confirmed the distinct particle size and distribution. (b) Evolution of the supported Pt nanoparticles radius during the thermal treatment. Distinct initial particle size and coverage entailed differences on the onset temperature for particle coarsening (II stage) to reach a similar evolution from 650 °C and above. (stage III). Error bars indicate 95 % of confidence.

the ALD Al_2O_3 layer on the sample stability and evolution can be clearly observed from the *in situ* data recorded, information that can be summarized as follows:

- Onset temperature for particle coarsening: when increasing the Al_2O_3 overcoat thickness, both samples presented a different behavior. The Pt-O sample showed a shift of the onset temperature for particle coarsening towards higher temperatures, extending the particle stability region. In fact, only 1 Al_2O_3 ALD cycle was enough for the Pt-O sample to increase considerably the stability window (575 °C up to ca. 730 °C). However, Pt-N samples showed only a slight augmentation of the temperature for starting the coarsening, even for a 40 ALD cycles overcoat layer, resulting in a similar onset than the as-deposited case without any capping layer (ca. 480 °C).

- Coarsening kinetics: the variation of the particle radius (ΔR) *versus* the temperature, i.e. the slope of the R(T) curve, decreases when increasing the overcoat thickness. In other words, a thicker layer of Al_2O_3 diminishes the kinetics of the coarsening process, since it would diminish the mobility of the PtO_x species that would be present on the surface, and hence, the kinetics of the coarsening process would be reduced.

- Coarsening reactivation: a higher temperature for PtO_x evaporation would be expected for a thicker Al_2O_3 layer. The presence of an overcoating layer of Al_2O_3 would help to prevent the PtO_x evaporation from the sample surface, disfavoring the particle coarsening reactivation. When increasing the number of Al_2O_3 ALD cycles (increasing thickness), the onset temperature for PtO_2 evaporation augments, and hence, the particle evolution does not follow the same trend (as the as deposited Pt-N and Pt-O sample did (Fig. 2b) whose onset temperature for coarsening reactivation was similar).

Scanning Electron Microscopy (SEM) images were acquired as proof of particle evolution in real space. Fig. S3 and Fig. S4 show representative quenches at different temperatures of the as deposited and 5 cycles overcoated Pt-O and Pt-N samples respectively. SEM images confirmed that 5 ALD cycles of Al_2O_3 on the Pt-O sample seemed to be enough to prevent particle coarsening up to 800 °C. However, the difference between the as-deposited and overcoated Pt-N sample was not so evident, since both cases presented a clear particle coarsening after the thermal treatment, in agreement with the *in situ* GISAXS data.

In situ data proved that the overcoating effect would depend on the initial particle situation: the smaller and closer the supported particles, the thicker the required Al_2O_3 layer to prevent particle coarsening. However, since the preparation procedure between Pt-O and Pt-N samples varies, an additional experiment was performed to evaluate the reproducibility and independence of the particle evolution on the ALD fabrication procedure for the supported Pt nanoparticles. Here, an as-deposited Pt-N sample was firstly annealed up to 600 °C in O_2 18 % in He, and then quenched to room temperature. Next, the sample was overcoated with 10 Al_2O_3 ALD cycles and annealed up to 850 °C while *in situ* GISAXS patterns were recorded. Fig. 4 depicts the *in situ* data recorded and the comparison with previous experiments. It was observed that the particle evolution extracted from the recorded GISAXS patterns followed the same trend than a previous annealed Pt-N sample (Fig. 3) when the first annealing profile was performed. After overcoating, the particle evolution during the second thermal treatment followed a similar R(T) evolution than the original Pt-O + 10 Al_2O_3 experiment.

This last experiment showed that: i) Process reproducibility: the repetition of two similar annealing experiments (i.e. Pt-N and

View Article Online
DOI: 10.1039/D0NR02444A

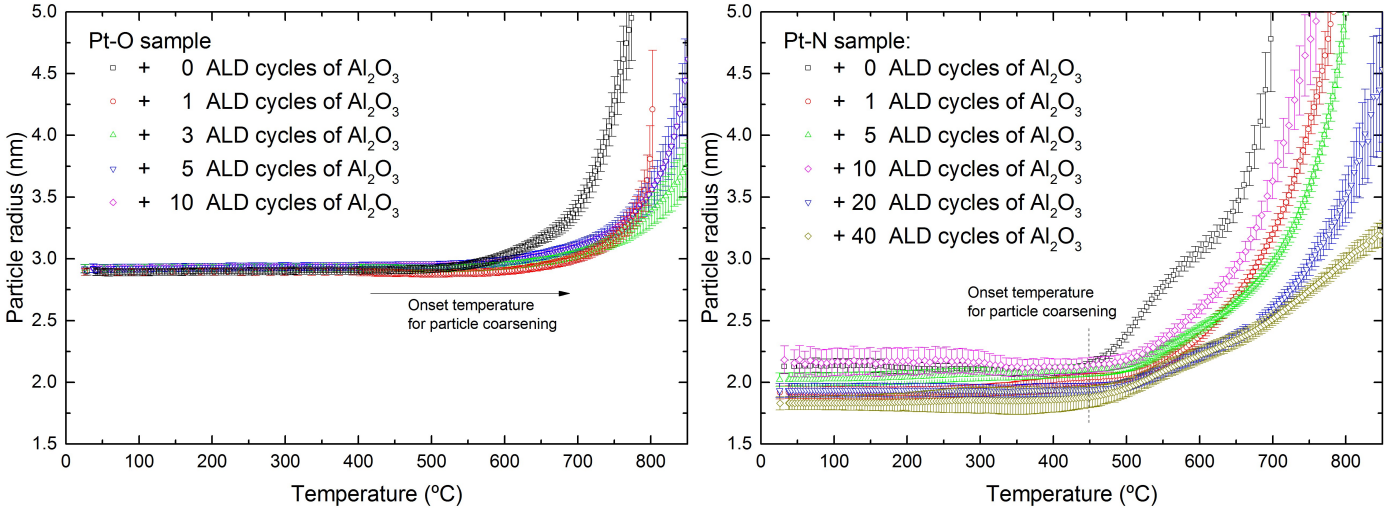

(a) Pt-O (b) Pt-N

Fig. 3 Evolution of the supported Pt nanoparticles radius during the annealing procedure (0.2 °C/s) in 18 % O_2 in He for the Pt-O (a) and Pt-N (b) samples. Error bars indicate 95 % of confidence.

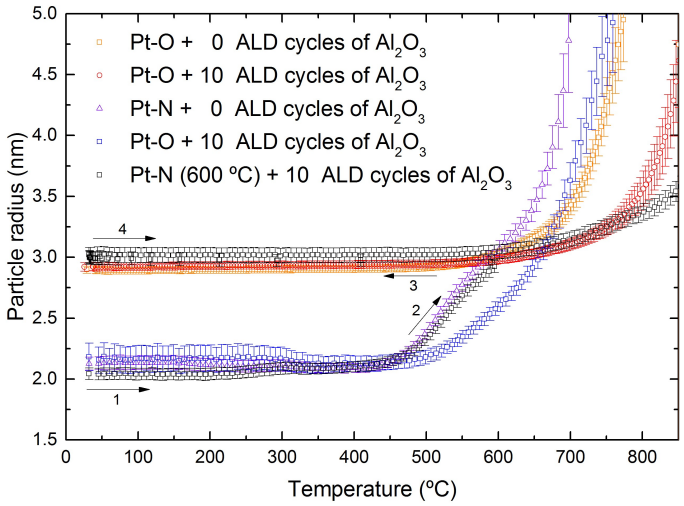

Fig. 4 Evaluation of particle evolution depending on the fabrication method. The as-deposited Pt-N sample was annealed up to 600 °C (1), quenched to room temperature and then overcoated with 10 cycles of Al_2O_3. Then, a new annealing procedure (2) was started, showing that the particle radius evolution followed the same trend than the original Pt-O + 10 cycles Al_2O_3 sample. Error bars indicate 95 % of confidence.

Pt-O + 10 Al_2O_3 cycles overcoat) with the new sample corroborated that the process is reproducible. ii) Size control via thermal annealing: by heating and quenching a sample with a given initial particle size, the final size could be modified towards larger particles by just a simple annealing experiment. iii) Fabrication methodology and thermal history: since the second thermal treatment after overcoating followed a similar R(T) evolution than the original Pt-O + 10 Al_2O_3 cycles experiment, results agree that the supported Pt nanoparticles behave similarly, independent of the sample thermal history and deposition procedure.

3.4 Low-energy ion scattering for Pt accessibility

Low-energy ion scattering (LEIS) measurements were performed to evaluate the surface elemental composition of some representative samples. LEIS is a scattering technique that only measures the top layer of atoms, which would also be accessible to molecules during a catalytic process. In this way, the *in situ* data can be correlated with the composition of the top-most surface layer. LEIS measurements were performed using a 3 keV He^+ beam for an overview of all elements, and an 8 keV Ar^+ beam for increased sensitivity to Pt.

Fig. 5(a) presents the 3 keV He^+ spectra, where the surface impurities can be evaluated. For instance, overcoated samples presented F contamination, which could have been produced during the overcoating process, since the as-deposited samples did not present any F characteristic signal. Moreover, a low intensity N peak was only present on the samples fabricated using N_2* as reactant, indicating that N remains as contaminant on the sample surface after the deposition process. LEIS results also allowed to observe the characteristic Al/Si peak (which cannot be resolved under these measurement conditions). This peak is of interest to evaluate the Pt surface coverage, especially for the non-overcoated samples where no Al should be present. The small Si signal on the as-deposited Pt-N sample proved that the 2 % of the surface was Si, showing that the Pt-N particles cover 98 % of the total substrate surface. This is in contrast to the as-deposited Pt-O sample, where a significant Si signal remains after the deposition, indicating a Pt coverage of 54 % of the sample. Therefore, LEIS data signaled that the Pt-N fabricated sample presented densely packed Pt nanoparticles, while the Pt-O process produced larger nanoparticles with a larger distance between neighboring nanoparticles. Additional measurements using Ar^+ at 8 keV were performed, being more sensitive to the Pt signal. Fig. 5(b) shows the additional measurements. The strongest Pt signal was in agreement with the previous data recorded with He^+ at 3 keV.

View Article Online
DOI: 10.1039/D0NR02444A

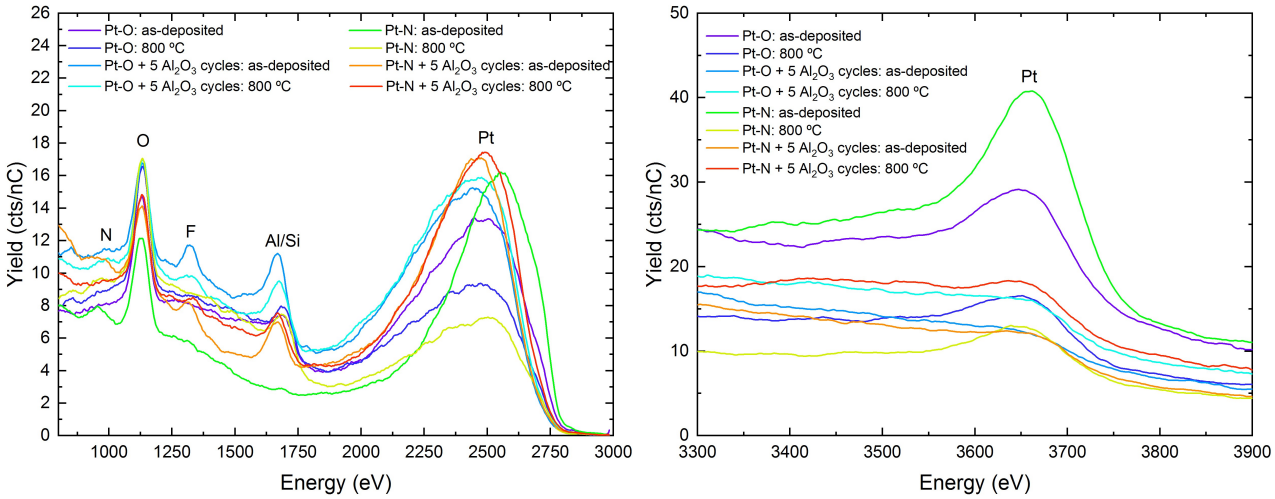

Fig. 5 LEIS spectra measured at 3 keV He^+ (a) and at 8 keV Ar^+ (b) of some representative samples.

Knowing that the Pt loading of the fabricated samples was comparable, it can be deduced that the larger the Pt signal in LEIS, the larger the amount of exposed Pt surface and hence, the smaller the nanoparticles. Therefore, the particle size for the different samples and deposition conditions could be compared. Moreover, LEIS enabled the possibility of obtaining quantitative information by modeling the spectra recorded. Table 2 presents the calculated results for the particle size and percentage of exposed Pt after LEIS background subtraction.

LEIS data showed that the Pt-O sample presented 54 % of Pt surface area with respect to the Pt-N sample. This difference in the Pt total surface coverage originated from the distinct nanoparticle size for the same noble metal loading: the Pt-O sample presented larger particles (radius of 3.6 nm) than the as deposited Pt-N (radius of 2.2 nm), which is in agreement with GISAXS results. Moreover, as deposited samples exhibited a diminishment of the Pt surface area after the annealing treatment to 800 °C, which was caused by an increase of the particle size due to the particle growth via coarsening. In this case, both Pt-N and Pt-O samples presented similar % of superficial Pt after annealing, being 25 and 29 % respectively, as expected for an equivalent particle radius of 4.2 and 4.4 nm for the Pt-N and Pt-O respectively. This result was in agreement with the recorded *in situ* GISAXS data, which demonstrated that both samples with similar Pt loading presented equivalent particle size at 800 °C. Overcoated samples showed a lower amount of superficial Pt right after the overcoating procedure without any thermal treatment, as expected due to the presence of Al_2O_3 covering the material. LEIS data (table 1) enabled the possibility to calculate the amount of overcoated Pt by comparing the exposed Pt for the as deposited and after overcoating, proving that ca. 86 % [82 %] of the Pt was covered with Al_2O_3 for the Pt-N [Pt-O] sample. After annealing, overcoated samples showed a clear difference when compared with the same sample before annealing: the Pt-O sample presented an augmentation of the amount of exposed Pt without any evidence of particle coarsening, while the Pt-N sample after overcoating and annealing also showed an increasing of the superficial Pt as well as an augmentation of the particle size. To understand this fact, *in situ* GISAXS results in combination with the LEIS calculated particle thickness have to be considered:

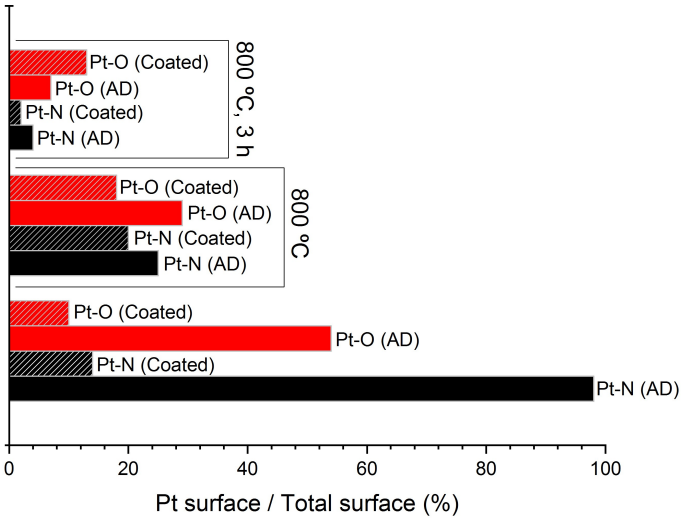

Fig. 6 Exposed Pt surface calculated by LEIS. The amount of exposed Pt decreases upon annealing, but proves to be higher for Pt-O overcoated particles than non-coated nanoparticles after a long isothermal annealing.

After overcoating the Pt-O sample with 5 Al_2O_3 ALD cycles, *in situ* GISAXS data proved that the aluminum oxide layer prevented the particle coarsening: after the annealing process up to 800 °C, the resulting particle size was similar to the initial state (as deposited situation), as also verified by SEM (Fig. S3) and LEIS particle thickness measurements (table 2). Contrarily, GISAXS data evidenced that 5 cycles of Al_2O_3 coating on the Pt-N sample was not enough to prevent particle coarsening, since the supported particles presented an increasing of the particle size during the thermal annealing, entailing a loss on the exposed Pt

View Article Online
DOI: 10.1039/D0NR02444A

Sample	Anneal	particle thickness (nm)	Exposed Pt[1] (%)
Pt-N	as-deposited	2.2 ± 0.1	98 ± 2
Pt-N	800 °C	4.2 ± 0.1	25 ± 2
Pt-N	800 °C (3h)	$> 8 \pm 0.1$	4 ± 2
Pt-N + 5 Al_2O_3 cycles	as-deposited	2.4 ± 0.1	14 ± 2
Pt-N + 5 Al_2O_3 cycles	800 °C	2.9 ± 0.1	20 ± 2
Pt-N + 5 Al_2O_3 cycles	800 °C (3 h)	$> 8 \pm 0.1$	2 ± 2
Pt-O	as-deposited	3.6 ± 0.1	54 ± 2
Pt-O	800 °C	4.4 ± 0.1	29 ± 2
Pt-O	800 °C (3h)	$> 8 \pm 0.1$	7 ± 2
Pt-O + 5 Al_2O_3 cycles	as-deposited	3.6 ± 0.1	10 ± 2
Pt-O + 5 Al_2O_3 cycles	800 °C	3.6 ± 0.1	18 ± 2
Pt-O + 5 Al_2O_3 cycles	800 °C (3h)	3.5 ± 0.1	13 ± 2

[1] Normalized amount of surface covered by Pt using the as-deposited Pt-N sample as reference.

Table 2 Overview of the results extracted from LEIS technique. It shows the amount of Pt on the surface normalized to the Pt-N, which showed a 98 % of Pt surface when compared with the Pt reference signal, meaning that lower values presented lower Pt surface area.

surface (Fig. S4). Nevertheless, it is worth to mention that when performing the annealing profile up to 800 °C, both overcoated samples showed an augmentation of the amount of exposed Pt after the process (LEIS data, table 2), which would probably be due to the Al_2O_3 layer cracking and porosity increase.

Furthermore, aiming to prove that the particle stability endures over time at high temperature, LEIS measurements (Fig. S5) were done on a sample subjected to the same 5 cycles of Al_2O_3 overcoat and thermal profile to 800 °C, but this time followed by an isothermal annealing of 3 h at 800 °C. Figure 6 summarizes the effect of overcoating on the amount of exposed Pt obtained by means of LEIS technique at the different process steps, i.e. as prepared, after annealed at 800 °C and after 3 h of isothermal annealing. This graph evidences a clear benefit of Al_2O_3 overcoating for particle coarsening prevention at high temperature, since the amount of exposed Pt for the Pt-O after an isothermal annealing at 800 °C was higher than for the same sample without overcoating, mainly due to the particle coarsening phenomenon. Fig. S6 corroborated the LEIS results, by showing in real space (SEM imaging) that the particle size for the overcoated Pt-O sample after the 3 h of isothermal annealing at 800 °C was similar to the as deposited case, contrarily to the Pt-N where a clear particle size increase was observed. These results proved the benefit of overcoating the sample with few ALD Al_2O_3 cycles to prevent particle coarsening and hence a diminishment of the exposed Pt surface area when high temperature applications are required.

Differences on the required amount of Al_2O_3 ALD cycles, and as consequence on the final overcoating layer thickness, are caused by the initial differences in particle distribution on the surface. Based on GISAXS and LEIS results, the Pt-O would present isolated nanoparticles that could be totally covered together with the interparticle Si substrate, while the physical particle isolation via Al_2O_3 overcoating for the Pt-N sample would be prevented because of the high areal density of supported nanoparticles. Results suggest the importance of having isolated nanoparticles for particle coarsening prevention using ALD overcoating: the efficiency of this singular methodology relies on the capability of physically isolating the supported nanoparticles on the surface, preventing the diffusion of species on the sample surface. Fig. 7

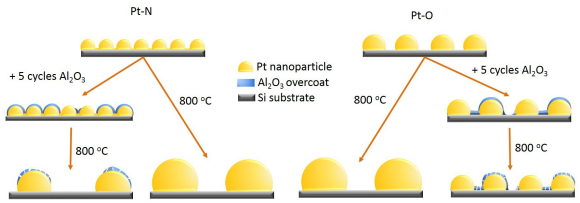

Fig. 7 Schematic representation of the particle evolution during the annealing treatment depending on the sample (i.e. Pt-N or Pt-O) and overcoating procedure.

schematically depicts the differences in the overcoat nature and particle evolution for both samples with and without overcoating protection layer, highlighting the efficiency of ALD overcoating for particle coarsening prevention.

4 Conclusions

Particle overcoating via Atomic Layer Deposition using Al_2O_3 as stabilizing layer has been demonstrated to prevent Pt particle coarsening during thermal annealing while allowing Pt surface accessibility for further applications. *In situ* synchrotron GISAXS results demonstrated that Al_2O_3 overcoating would require isolated nanoparticles for an effective particle stability under the harsh thermal and environmental conditions investigated: while a single ALD cycle of Al_2O_3 deposition proved to increase the temperature for particle coarsening of isolated Pt nanoparticles on the surface, larger number of cycles did not achieve the same stabilization when nanoparticles are densely packaged. Furthermore, LEIS proved the Pt surface accessibility of all the samples even after Al_2O_3 overcoating, which is of interest for catalytic applications, also demonstrating that the Pt accessibility augments during the thermal treatment. After a long isothermal annealing, a sample with overcoat outperformed a sample without overcoat in terms of Pt accessibility, proving the effectiveness of the stability overcoat. In conclusion, ALD overcoating is an effective tool for preventing particle coarsening while applying harsh thermal and environmental conditions to supported nanoparticles, with limitations for the denser and connected nanoparticles. This stability strategy could be extended to other systems due to the high effec-

View Article Online
DOI: 10.1039/D0NR02444A

tiveness of Al_2O_3 ALD overcoating over a wide range of materials and supports.

5 Conflicts of interest

There are no conflicts to declare.

6 Acknowledgments

The authors acknowledge the FWO-Vlaanderen for financing beam time at the DUBBLE beamline of the ESRF and the associated travel costs. We also thank CALIPSO (European Community's Trans National Access Program) for covering the associated costs of the beamtime at SOLEIL synchrotron. We also thank to the SOLEIL and ESRF synchrotron staff for smoothly running the facilities. J.D., T.D., K.V.K and M.M.M. acknowledge the FWO for a research fellowship. The research leading to these results has received funding from the FWO-Vlaanderen, BOF-UGent (GOA 01G01513) and Hercules foundation (AUGE/09/014).

Notes and references

1 A. M. Gänzler, M. Casapu, P. Vernoux, S. Loridant, F. J. Cadete Santos Aires, T. Epicier, B. Betz, R. Hoyer and J. D. Grunwaldt, *Angew. Chemie - Int. Ed.*, 2017, **56**, 13078–13082.

2 U. G. Vej-Hansen, M. Escudero-Escribano, A. Velázquez-Palenzuela, P. Malacrida, J. Rossmeisl, I. E. L. Stephens, I. Chorkendorff and J. Schiøtz, *Electrocatalysis*, 2017, **8**, 594–604.

3 N. Cheng, S. Stambula, D. Wang, M. N. Banis, J. Liu, A. Riese, B. Xiao, R. Li, T. K. Sham, L. M. Liu, G. A. Botton and X. Sun, *Nat. Commun.*, 2016, **7**, 1–9.

4 T. Imaoka, Y. Akanuma, N. Haruta, S. Tsuchiya, K. Ishihara, T. Okayasu, W. J. Chun, M. Takahashi and K. Yamamoto, *Nat. Commun.*, 2017, **8**, 1–8.

5 Z. Weng and F. Zaera, *Top. Catal.*, 2019.

6 L. Li, L. Hu, J. Li and Z. Wei, *Nano Res.*, 2015, **8**, 418–440.

7 Y. Lykhach, A. Bruix, S. Fabris, V. Potin, I. Matolínová, V. Matolín, J. Libuda and K. M. Neyman, *Catal. Sci. Technol.*, 2017, **7**, 4315–4345.

8 K. M. Bratlie, H. Lee, K. Komvopoulos, P. Yang and G. A. Somorjai, *Nano Lett.*, 2007, **7**, 3097–3101.

9 C. H. Choi, M. Kim, H. C. Kwon, S. J. Cho, S. Yun, H. T. Kim, K. J. Mayrhofer, H. Kim and M. Choi, *Nat. Commun.*, 2016, **7**, 1–9.

10 K. Ding, A. Gulec, A. M. Johnson, N. M. Schweitzer, G. D. Stucky, L. D. Marks and P. C. Stair, *Science (80-.).*, 2015, **350**, 189–192.

11 E. Solano, J. Dendooven, M. M. Minjauw, R. K. Ramachandran, K. Van De Kerckhove, T. Dobbelaere, D. Hermida-Merino and C. Detavernier, *Nanoscale*, 2017, **9**, 13159–13170.

12 F. Grillo, J. A. Moulijn, M. T. Kreutzer and J. R. van Ommen, *Catal. Today*, 2018, 1–11.

13 C. Lafforgue, A. Zadick, L. Dubau, F. Maillard and M. Chatenet, *Fuel Cells*, 2018, 229–238.

14 Y. Dai, P. Lu, Z. Cao, C. T. Campbell and Y. Xia, *Chem. Soc. Rev.*, 2018, 4314–4331.

15 C. Dong, C. Lian, S. Hu, Z. Deng, J. Gong, M. Li, H. Liu, M. Xing and J. Zhang, *Nat. Commun.*, 2018, **9**, 1–11.

16 J. Jones, H. Xiong, A. T. DeLaRiva, E. J. Peterson, H. Pham, S. R. Challa, G. Qi, S. Oh, M. H. Wiebenga, X. I. P. Hernández, Y. Wang and A. K. Datye, *Science (80-.).*, 2016, **353**, 150–154.

17 K. Koizumi, K. Nobusada and M. Boero, *Chem. - A Eur. J.*, 2017, **23**, 1531–1538.

18 D. Y. Chung, J. M. Yoo and Y. E. Sung, *Adv. Mater.*, 2018, **1704123**, 1–20.

19 J. Liu, Q. Ji, T. Imai, K. Ariga and H. Abe, *Sci. Rep.*, 2017, **7**, 1–8.

20 L. Liu, M. Lopez-Haro, C. W. Lopes, C. Li, P. Concepcion, L. Simonelli, J. J. Calvino and A. Corma, *Nat. Mater.*, 2019.

21 H. H. K. P. C. S. Junling Lu, Baosong Fu, Mayfair C. Kung, Guomin Xiao, Jeffrey W. Elam, *Science (80-.).*, 2009, **335**, 105–1208.

22 B. J. O'Neill, C. Sener, D. H. K. Jackson, T. F. Kuech and J. A. Dumesic, *ChemSusChem*, 2014, **7**, 3247–3251.

23 T. J. Schwartz, B. J. O'Neill, B. H. Shanks and J. A. Dumesic, *ACS Catal.*, 2014, **4**, 2060–2069.

24 B. J. O'Neill, D. H. K. Jackson, J. Lee, C. Canlas, P. C. Stair, C. L. Marshall, J. W. Elam, T. F. Kuech, J. A. Dumesic and G. W. Huber, *ACS Catal.*, 2015, **5**, 1804–1825.

25 Z. Bo, S. Ahn, M. A. Ardagh, N. M. Schweitzer, C. P. Canlas, O. K. Farha and J. M. Notestein, *Appl. Catal. A Gen.*, 2018, **551**, 122–128.

26 Y. Gong, D. Palacio, X. Song, R. L. Patel, X. Liang, X. Zhao, J. B. Goodenough and K. Huang, *Nano Lett.*, 2013, **13**, 4340–4345.

27 A. S. Asundi, J. A. Raiford and S. F. Bent, *ACS Energy Lett.*, 2019, **4**, 908–925.

28 J. Lu, B. Liu, J. P. Greeley, Z. Feng, J. A. Libera, Y. Lei, M. J. Bedzyk, P. C. Stair and J. W. Elam, *Chem. Mater.*, 2012, **24**, 2047–2055.

29 A. Meyer, N. Franz, H. P. Oepen, J. Perlich, G. Carbone and T. H. Metzger, *Nano Res.*, 2017, **10**, 456–471.

30 J. Dendooven, R. K. Ramachandran, E. Solano, M. Kurttepeli, M. M. Minjauw, T. Dobbelaere, K. Devloo-Casier, A. Vantomme, S. Bals, G. Portale, A. Coati and C. Detavernier, *Nat. Commun.*, 2017, **8**, 1074.

31 G. Renaud, R. Lazzari, C. Revenant, A. Barbier, M. Noblet, O. Ulrich, F. Leroy, J. Jupille, Y. Borensztein, C. R. Henry, J.-P. Deville, F. Scheurer, J. Mane-Mane and O. Fruchart, *Science (80-.).*, 2003, **300**, 1416–1419.

32 G. Renaud, R. Lazzari and F. Leroy, *Surf. Sci. Rep.*, 2009, **64**, 255–380.

33 J. Dendooven, E. Solano, M. M. Minjauw, K. V. D. Kerckhove, A. Coati, E. Fonda, G. Portale, Y. Garreau and C. Detavernier, *Rev. Sci. Instrum.*, 2016, **87**, 113905.

34 J. F. Ziegler, U. Littmark and J. P. Biersack, *The stopping and range of ions in solids*, Pergamon New York, 1985.